Hydrol. Earth Syst. Sci. Discuss., 10, 4301–4335, 2013
www.hydrol-earth-syst-sci-discuss.net/10/4301/2013/
doi:10.5194/hessd-10-4301-2013

Hydrology and Earth System Sciences
Open Access
Discussions

Space-time kriging extension of precipitation variability at 12 km spacing from tree-ring chronologies and its implications for drought analysis

F. Biondi

DendroLab, Mackay School of Earth Sciences and Engineering, University of Nevada, Reno, NV 89557, USA

Received: 20 February 2013 – Accepted: 25 March 2013 – Published: 5 April 2013

Correspondence to: F. Biondi (franco.biondi@gmail.com)

Published by Copernicus Publications on behalf of the European Geosciences Union.

Abstract

Understanding and preparing for future hydroclimatic variability greatly benefits from long (i.e., multi-century) records at seasonal to annual time steps that have been gridded at km-scale spatial intervals over a geographic region. Kriging is a geostatistical technique commonly used for optimal interpolation of environmental data, and space-time geostatistical models can improve kriging estimates when long temporal sequences of observations exist at relatively few points on the landscape. Here I present how a network of 22 tree-ring chronologies from single-leaf pinyon (*Pinus monophylla*) in the central Great Basin of North America was used to extend hydroclimatic records both temporally and spatially. First, the Line of Organic Correlation (LOC) method was used to reconstruct October–May total precipitation anomalies at each tree-ring site, as these ecotonal environments at the lower forest border are typically moisture limited. Individual site reconstructions were then combined using a hierarchical model of spatio-temporal kriging that produced annual anomaly maps on a 12 × 12 km grid during the period in common among all chronologies (1650–1976). Hydro-climatic episodes were numerically identified and modeled using their duration, magnitude, and peak. Spatial patterns were more variable during wet years than during dry years, and the evolution of drought episodes over space and time could be visualized and quantified. The most remarkable episode in the entire reconstruction was the early 1900s pluvial, followed by the late 1800s drought. The 1930s "Dust Bowl" drought was among the top ten hydroclimatic episodes in the past few centuries. These results directly address the needs of water and natural resource managers with respect to planning for "worst case" scenarios of drought duration and magnitude at the watershed level. For instance, it is possible to analyze which geographical areas are more likely to be impacted by severe and sustained droughts at annual or multiannual timescales and at spatial resolutions commonly used by regional climate models.

HESSD
10, 4301–4335, 2013

1 Introduction

Climate variability and change can influence multiple hydrologic characteristics, such as the proportion of snowfall vs. rainfall (Knowles et al., 2006), the occurrence of droughts and floods (Cayan et al., 1999; Redmond et al., 2002), the timing of peak runoff (Stewart et al., 2004), and the amount of storage in reservoirs (Barnett and Pierce, 2008; Barsugli et al., 2009). One strategy available to water managers for understanding (and coping with) the risk associated with these future impacts is to obtain a clear definition of past hydrological variability and extremes (Stakhiv, 2011). In the western United States, as well as in other parts of the world, water resources are vulnerable to climate fluctuations (e.g., Rajagopalan et al., 2009; Seager et al., 2007), but instrumental records of precipitation, temperature, and surface-water flow are spatially and temporally limited, with length rarely exceeding the past few decades. At the same time, this region is rich with proxy records of hydroclimatic variables derived from tree rings (Loaiciga et al., 1993), given a unique combination of steep topography and semi-arid conditions that limit wood formation, presence of old trees at both lower and upper treelines, and a large body of ecological research on the climate sensitivity of these species (Fritts, 1976; Speer, 2010).

Blending instrumental and proxy records together with projected climate model simulations to inform water resource management is a topic that has received some attention (Gray and McCabe, 2010; Prairie et al., 2008), but requires additional studies, as suggested in a joint report by the Bureau of Reclamation and United States Army Corps of Engineers (Brekke, 2011). In the Great Basin of North America, dendroclimatic reconstructions of moisture parameters have a long and productive history, starting with pioneering work in the 1930s (Antevs, 1938; Hardman and Reil, 1936), continuing with isolated efforts into the 1980s (Nichols, 1989; Smith, 1986), and arriving at the development of extremely long (> 1000 yr) proxy records of precipitation in more recent times (Gray et al., 2004; Hughes and Graumlich, 1996; Knight et al., 2010). A systematic, spatially gridded set of drought reconstructions derived from tree-ring chronologies

HESSD
10, 4301–4335, 2013

(Cook et al., 2004) also included millennia-long time series for Nevada, although at the relatively coarse scale of 2.5° of latitude and longitude (Cook and Krusic, 2003). Besides an overall arid to semi-arid continental climate (Houghton et al., 1975), the Great Basin of North America is characterized by an upper and a lower treeline, with the latter being occupied by pinyon-juniper woodlands (West and Young, 2000). These ecosystems (Nevada's "pigmy forest") are dominated by single-leaf pinyon (*Pinus monophylla* Torr. and Frém.) and Utah juniper (*Juniperus osteosperma* (Torr.) Little), and characterized by a continental semi-arid climate with total annual precipitation usually between 300 and 500 mm falling mostly during the cool season, and a frost-free period ranging from ∼ 90 to ∼ 200 days. Single-leaf pinyon, the only one-needle pine in the world, can therefore survive both extreme drought and severely cold climate, and currently covers about 67 845 km^2 (Cole et al., 2008), although its distribution has increased rapidly since Euro–American settlement (Romme et al., 2009), continuing a trend present throughout the Holocene (see Fig. 16 of chapter 8 in Grayson, 2011).

Among the many interpolation techniques available to produce gridded datasets from sparse point locations (Tabios III and Salas, 1985), geostatistical techniques such as kriging have various advantages (Biondi et al., 1994). In particular, kriging is the best linear unbiased estimator of the regionalized variable at unsampled locations, because it is constrained to produce residuals with zero mean and minimal variance (Isaaks and Srivastava, 1989). In recent times there has been increased interest in using space-time geostatistical models to improve spatial estimation when long temporal sequences of observations exist at relatively few points on the landscape (Christakos, 2000). Since the empirical estimation of space-time covariance models can become highly complex, many studies assume both spatiotemporal stationarity and the separability of spatial and temporal components (Kyriakidis and Journel, 1999). These assumptions have been justified by arguing that no clear distance metric exists in space-time as there is in Euclidean space, given that time is ordered and unidirectional, while physical space is not. Recent developments have relaxed the separability assumption by introducing hierarchical models, estimated using Bayesian or empirical approaches (Cressie

HESSD
10, 4301–4335, 2013

and Wikle, 2011). In this framework, multivariate approaches can account for spatio-temporal covariates and nonstationarity (Fassó and Cameletti, 2010). So, for instance, elevation can be entered as a covariate in order to compute a single kriging estimate for each two-dimensional grid point location rather than predict over all possible altitudes (Fassó and Cameletti, 2009).

Increased spatial resolution is a necessity when simulating hydroclimatic processes in topographically complex terrain (Hijmans et al., 2005). With respect to water resources, Hoerling et al. (2009) found that using data spatially interpolated on 4 or 12 km grid cells improved agreement among models used for estimating future river runoff in the Colorado River basin, whose management is a vital issue for the western USA (National Research Council, 2007). When long proxy records of climate exist at relatively sparse locations, the combination of temporal and spatial autocorrelation structures through space-time kriging provides an effective method for producing gridded proxy records at the same spacing as regional climate models and statistical downscaling techniques. I present here an example of how tree-ring records developed from single-leaf pinyon trees in the eastern Great Basin (Biondi and Strachan, 2005) and calibrated against PRISM data (Daly et al., 1994) to extend precipitation records, could be interpolated by year at 12 km grid increments, which are easily comparable with downscaled regional climate simulations. The study had mainly a hydrological focus, as it tested if instrumental representations of severe droughts (such as the 1930s one) could be augmented by much longer proxy records, while also investigating the spatial features of climatic episodes, i.e., dry and wet spells, that have occurred over the past few centuries.

2 Materials and methods

A network of 22 tree-ring chronologies (Fig. 1) located in the eastern portion of Nevada and spanning 114.0–116.0° W longitude and 37.5–39.8° N latitude, was used to extend precipitation records. Data collection followed standard dendrochronological

HESSD
10, 4301–4335, 2013

procedures, with 4.3 mm-wide increment cores taken from individual trees at or near breast height, and from opposite sides of the tree along slope contours whenever possible (Grissino-Mayer, 2003). Site locations were decided based on presence of old, healthy individuals of single-leaf pinyon. Wood cores were stored and dried inside paper straws in the field, then transported to the laboratory, where they were glued to grooved wood mounts, progressively sanded (first mechanically, then by hand) until individual cells were clearly visible under a binocular stereo-zoom microscope with 10–50 × magnification. All crossdating (Stokes and Smiley, 1996) and locally absent ring assignment was done visually using a binocular microscope prior to ring width measurement on a Velmex stage with 1 µm resolution. The ring-width measurement data were then evaluated using the software program COFECHA (Grissino-Mayer, 2001; Holmes, 1983). Most sites were sampled in 2008-'09 by DendroLab personnel, but a few existing chronologies for the study area that are in the public domain were also collected from the International Tree-Ring Data Bank (ITRDB; Grissino-Mayer and Fritts, 1997). Most ITRDB collections were completed decades ago, and their inclusion in the dataset is not a guarantee of quality. For instance, the oldest tree-ring collection for pinyon in Nevada (id 043630) was not used because it listed "Pinus edulis" (the Colorado or southwestern pinyon) as the species. Another *Pinus monophylla* chronology (id 461639) was excluded because it was less than 150 yr long, considerably shorter than expected given the longevity of the species.

The next step in the analysis combined all measurements for a site and species into a single "master" tree-ring chronology (Fritts, 1976). This process requires that we "standardize" the ring-width measurements, because tree radial growth is a result of individual biological and ecological processes, and it is necessary to minimize age-related trends and other non-climatic variability prior to combining multiple ring-width series together (Cook and Kairiukstis, 1990). A cubic smoothing spline (Cook and Peters, 1981) was fit to each ring-width series to avoid known issues that affect other types of standardization functions, such as modified negative exponentials (Biondi and Qeadan, 2008b). Ring indices were obtained as ratios between the ring-width

HESSD
10, 4301–4335, 2013

measurements and the corresponding spline values. The median of all indices available for a year was used to produce the chronology value for that year, as follows:

$$\bar{I}_t = \underset{i=1,\ldots,n_t}{\text{median}} \left(\frac{w_t}{y_t} \right)_i \quad (1)$$

where $\bar{I}_t$ = chronology value in year t = median annual index; n_t = number of samples in year t, with $n_t \geq 3$; w = crossdated ring width (mm, with 1000th digit resolution) of sample i in year t; y = value of sample i in year t computed by fitting a cubic smoothing spline with 50 % frequency response at a period of 100 yr to ring width series i; w_t/y_t = dimensionless index value of sample i in year t. ITRDB ring-width measurements were also standardized using this formula. Numerical analyses were performed using a combination of in-house scripts for SAS (Delwiche and Slaughter, 2003) and the R numerical computing package (R Development Core Team, 2012), together with task-specific software, either stand-alone (Biondi and Waikul, 2004) or modular (Bunn et al., 2012).

Calibration of dendroclimatic records with instrumental data was done using interpolated and spatially averaged records, i.e., respectively PRISM (Daly et al., 1994) and Climate Division (Guttman and Quayle, 1996) data. PRISM monthly total precipitation, mean minimum and mean maximum air temperature from 1895 to 2006 at 2.5 arc-minute grid spacing were downloaded from the DendroLab ArcIMS web server *DendroNet GIS* (http://www.dendrolab.org/GIS/) by clicking on the map grid cell that included the coordinates for a tree-ring site. The average annual cycle for these three instrumental variables was computed using all 22 PRISM cells. Monthly total precipitation and mean air temperature for Nevada Climate Divisions 2 and 3 during 1895–2006 were downloaded from the NOAA/NCDC website (ftp://ftp.ncdc.noaa.gov/pub/data/cirs/) for comparison with PRISM data. Time-series patterns of average PRISM and Climate Division instrumental records were plotted by year using two seasonal combinations: (a) cool and wet: October–May; and (b) warm and dry: June–September.

HESSD
10, 4301–4335, 2013

Statistical relationships between each tree-ring chronology and PRISM monthly climate data were investigated for the water year (October–September) using bootstrapped correlation and response functions (Biondi, 1997). Based on the average climate regime at the study sites and on the main climatic signals in the tree-ring chronologies, our target for record extension was the total October–May precipitation. When the correlation between a tree-ring chronology and the local PRISM precipitation was less than 0.4, the reconstruction was not performed. The "Line of Organic Correlation" (LOC) method (Helsel and Hirsch, 2002) was used for record extension to better represent uncertainty in the underlying processes (Biondi et al., 2010). LOC relies on minimizing not the sum of squared distances (either vertical or horizontal) from the final regression line, but rather the area of all triangles formed by the horizontal and vertical distance to the regression line. It is therefore also known as least areas regression, but it has been called standardized (or reduced) major axis regression, least products regression or diagonal regression. In hydrology, the LOC method is known as the "maintenance of variance extension" (MOVE; Salas et al., 2008), and its main advantage is that the cumulative distribution function of the reconstructed values, including the variance and probabilities of extreme events (both dry and wet), resembles the distribution of the instrumental data used for calibration. The LOC method was evaluated in detail for a reconstruction of streamflow variability in the Cleve Creek watershed (Strachan et al., 2012). Since the LOC method was used for reconstructing past variability together with wet and dry episodes, it produced a proxy climate record with an overall mean of zero, while deviations above and below this reference level (i.e., anomalies) had physical units (mm in this case).

I performed space-time estimation of tree-ring derived precipitation for grid cells comparable to those used for downscaled climate projections and model output from PRISM and regional climate models. Two different geostatistical approaches were used to quantify relationships and to develop gridded records at 12 km intervals. One approach was based on a hierarchical model (Cressie and Wikle, 2011) that combines a data model (i.e., the probability distribution of the data given a hidden true process)

HESSD
10, 4301–4335, 2013

with a process model (i.e., the probability distribution of the hidden process) to provide a conditional probability distribution of the hidden process given the data (the "posterior" of Bayesian statistics). Another approach was based on the linear combination of spatial and temporal autocorrelation structures, essentially considering time as an additional dimension with unidirectional features (Kyriakidis and Journel, 1999). The two methods were compared using the R software environment: a separable (product-sum) exponential covariance model was applied using the gstat package (Pebesma, 2013), while hierarchical modeling was implemented using the Stem package (Fassó and Cameletti, 2009). The tree-ring reconstructions were stationary in time, and spatial structures were considered to be isotropic. Given the importance of orographic precipitation in the Great Basin (Houghton et al., 1975), elevation was entered as a covariate in the hierarchical model in order to compute a single kriging estimate for each two-dimensional grid point location, rather than predict over all possible altitudes, as would have been necessary in gstat. Since no missing values were allowed, the period 1650–1976 was selected to include 17 DendroLab chronologies and 5 ITRDB chronologies that effectively improved spatial coverage in the basins of interest; spatio-temporal patterns post-1976 are available from instrumental records.

The average of all grid point estimates of October–May precipitation was computed by year to obtain a single time series that could be analyzed in terms of episode duration, magnitude, and peak (Biondi et al., 2008). Duration is the number of time intervals (e.g., years) the process remains continuously above (or below) a reference level. Magnitude is the sum of all series values for a given duration, hence it is equivalent to the area under (or above) the reference level. Episodes above (or below) a reference level are usually called positive (or negative). Analysis of episode parameters allows a less subjective identification of the "strongest", "greatest", or "most remarkable" periods, and although this approach is normally used for drought analysis, it can be applied to any cumulated deviations (Biondi et al., 2002). Each episode parameter was ranked separately, and the three ranks were added to obtain the final episode score; the higher the score, the stronger the episode.

HESSD
10, 4301–4335, 2013

3 Results

The 22 tree-ring chronologies (Table 1) were distributed over 500 m of elevation (~ 1930–2430 m) and a geographical area about 50 % longer in the N–S direction (~ 230 km) than in the E–W direction (~ 155 km). Crossdated tree ages reached a maximum of 784 yr, and mean segment length ranged from 192 to 443 yr, with an average of 326 yr. Because of the high tree longevity and large number of samples per site (32 on average), this dendrochronological network comprised a total of 219 265 crossdated ring-width measurements – roughly a mean of ten thousand measurements per site. Locally absent rings were numerous, ranging from 1.2 to 5.5 % of the total number of measurements per site, with an average of 3 %. Mean pairwise correlation between tree-ring chronologies during 1650–1976 was 0.7, and for that period the first principal component accounted for 70 % of the total variance. In agreement with their numerical similarity, tree-ring chronologies showed highly coherent time-series patters (Fig. 2), especially during major droughts, such as the late 1500s (Stahle et al., 2000) and the 1930s "Dust Bowl" (Fye et al., 2003). The chronologies also showed a high level of variability, as indicated by their large standard deviation (from 0.292 to 0.467, with a mean of 0.359) and small lag-one autocorrelation (from 0.033 to 0.345, with a mean of 0.213). For comparison, Fritts and Shatz (1975) reported that 11 chronologies of southwestern pinyon (*Pinus edulis*) had higher standard deviation (mean of 0.395) and lag-one autocorrelation (mean of 0.361), although different standardization options and historical periods may have contributed to these dissimilarities. Rather than using mean sensitivity, which refers only to adjacent rings, the all-lag sensitivity of the chronologies was quantified by the Gini coefficient (Biondi and Qeadan, 2008a). Its values (from 0.166 to 0.271, with a mean of 0.206) were higher than those previously reported for the same species, and would have fallen right below those calculated for *Pinus edulis* during the 1880–1960 period (see Fig. 2 in Biondi and Qeadan, 2008a), most likely because of the different standardization option used in this analysis.

HESSD
10, 4301–4335, 2013

Climate regime at the study areas was quantified by month (Fig. 3). The annual cycle of precipitation showed higher values and greater variability (especially from February through April) if PRISM data, rather than climate division ones, were used. Since PRISM data referred to more local conditions, and were restricted to mountain areas (mean elevation of tree-ring sites was 2280 m), temperatures were also cooler, especially from April to July. Despite these differences in absolute values, temporal changes were quite uniform (Fig. 4), as also suggested by extremely high correlations from 1895 to 2006 between PRISM and divisional precipitation ($r = 0.9$, p value < 0.0001, in both seasons) as well as temperature ($r = 0.9$, p value < 0.0001, for October–May, and $r = 0.8$, p value < 0.0001, for June–September). In terms of overall trends, the divisional data showed a slight temperature increase over time ($r = 0.4$, p value < 0.0001), which was less evident in the PRISM data ($r = 0.3$, p value < 0.01). Finally, warm-season precipitation and temperature were inversely correlated in both datasets ($r = -0.3$ to -0.4), and a slight negative correlation (-0.2, p value < 0.05) also existed between precipitation in October–May and temperature during the following months (June–September). Since the PRISM data better captured the climatic regime at the study areas, and at the same time they were extremely similar to the divisional data in terms of year-to-year patterns, they were then used for proxy calibration and reconstruction purposes.

A pooled spatio-temporal variogram was calculated as the average of 327 annual variograms for the 22 point reconstructions (Pebesma, 2013). An appropriate model for the pooled variogram was given by a nugget plus exponential term with a range of about 100 km, and a sill that was about 75 % of the combined spatial variance (Fig. 5). Most of the spatial dependence was not temporally lagged, with very little spatial dependence for temporal lags greater than one (Fig. 6). A spatial range of 100 km and time range of 1 yr was therefore used for space-time kriging interpolation. The three driest years identified using an average of the gstat gridded values are the same as those calculated from an average of the Stem interpolation: 1934, 1782, and 1879. Similarly, the three wettest years were the same when results were averaged using one or the other method: 1726, 1914, and 1868. The spatial patterns, however, were not

HESSD
10, 4301–4335, 2013

the same, as the non-hierarchical interpolation varied less over the study area in any given year, most likely because it did not incorporate elevation as an additional factor. Further analyses were therefore based on gridded values produced by the hierarchical method using the Stem package, which are shown year-by-year in Fig. 7.

As mentioned above, the three worst annual droughts in the 327 yr record were 1934 (mean anomaly of −181 mm, 3.1 standard deviations below the zero reference level), 1782 (mean anomaly of −171 mm, 3.0 standard deviations below normal), and 1879 (mean anomaly of −150 mm, 2.6 standard deviations below normal). Although the entire study region experienced a drought in those years, the intensity of each event varied spatially (Fig. 8), and the availability of values on a 12 km grid would allow for detailed analyses of individual subwatersheds. Similarly, the three wettest years, 1726 (mean anomaly of 156 mm, 2.7 standard deviations above the zero reference level), 1914 (mean anomaly of 140 mm, 2.4 standard deviations above normal), and 1868 (mean anomaly of 130 mm, 2.3 standard deviations above normal) occurred with different geographical features (Fig. 8). Furthermore, as can be seen particularly well in Fig. 8, wet years were usually more spatially variable than dry years: the bottom row is characterized by three distinct patterns (from left to right: U-shaped, C-shaped, and reverse-L-shaped), while the top row displays a more homogeneous spatial arrangement (roughly an east-west dipole). The time series of the total October–May precipitation anomaly obtained by averaging the 315 space-time kriging values (Fig. 9) was almost perfectly correlated ($r = 0.997$) with the mean of the 22 proxy point reconstructions, but some of the rankings were different. For example, the third wettest year was 1838 (with 1868 immediately following) instead of 1868 (with 1838 immediately following). Because of this similarity, and of the higher spatial representation provided by the mean of the interpolated values, episode analysis was performed using the average of the 315 grid points.

A total of 150 wet and dry episodes were identified in the 327 yr record of proxy October–May total precipitation anomalies (Table 2a). Episode duration ranged from 1 to 11 yr, and the longest interval was 1905–1915 (an 11 yr wet spell), followed by

HESSD
10, 4301–4335, 2013

two 8 yr long episodes, one dry (1876–1883) and one wet (1848–1855). The greatest magnitude also belonged to the early 1900s pluvial (1905–1915), followed by another wet period (1723–1728) and by a dry one (1706–1710). The strongest peak occurred during the "Dust Bowl" drought (1933–1936 in this record), followed by another dry episode (1780–1783), and then by the wet spell that also had the second largest magnitude (1723–1728). According to a simple scoring rule (Table 2), the most remarkable episode was the early 1900s pluvial (1905–1915), followed by the late 1800s drought (1876–1883). The 1930s "Dust Bowl" drought (1933–1936) was in 8th position, making it an important episode over the past few centuries, as was also found for this part of the Great Basin when reconstructing Cleve Creek streamflow over the past 550 yr (Strachan et al., 2012). To capture interannual variability mostly associated with the ENSO (El Niño-Southern Oscillation) phenomenon (Cayan et al., 1999), the annual precipitation anomalies were smoothed with a cubic spline having a 50 % frequency response at a 7.5 yr period (Cook and Peters, 1981). This new time series (Fig. 9) was comprised of 55 episodes (Table 2b), among which the early 1900s pluvial (1904–1924) remained the strongest one, and was then followed by five dry spells, starting with the 1930s "Dust Bowl" (1925–1937) as the second most remarkable episode, and including the 1950s drought (1946–1964) in fifth position.

4 Discussion

Spatially interpolated climate data on regular grids are routinely employed for research and management purposes in a number of disciplines, including ecological (Guisan and Thuiller, 2005), agricultural (Daly et al., 2008), and social (Wilby, 2007) sciences. The widespread distribution of single-leaf pinyon in ecotonal and fire-protected conditions throughout the Great Basin allowed for the development of a moisture-sensitive tree-ring network spanning the past few centuries. Applying space-time kriging to obtain dendroclimatic records of precipitation interpolated by year at 12 km grid increments should then substantially enhance their management implications, as these

HESSD
10, 4301–4335, 2013

"dendroclimatic surfaces" are one of the sources of information being studied by Southern Nevada Water Authority to estimate the impacts of prolonged droughts in this region (Abatzoglou et al., 2012). In terms of year-by-year patterns, spatial variability was generally higher during wet years than during dry ones, and further research will be aimed at more formally quantifying such differences. For now it is clear that the mean of the 22 individual reconstructions and the mean of the 315 grid-point reconstructions showed essentially the same variability, hence spatial patterns themselves were the most important result derived from space-time kriging of site-specific records. In other words, the true value of km-scale climate fields is the fine-grain spatial representation of dry and wet episodes, since their average temporal evolution over the landscape can be captured by a relatively limited set of points.

In fact, reconstructed time series patterns can often be compared in paleoclimatic studies across fairly distant regions because of their coarse spatial resolution. As an example, the area-averaged precipitation anomalies (Fig. 9) were compared to other dendroclimatic reconstructions that had been archived at the NOAA/NGDC Paleoclimatology Program. Total annual (from previous July to current June) precipitation for Nevada Climate Division 3 (Hughes and Graumlich, 2000) as well as total annual (from previous June to current June) precipitation for Utah Climate Division 6 (Gray et al., 2005) provided two records of precipitation from areas located near the study region, although the former includes a much larger section of the Great Basin, extending west all the way to the Sierra Nevada (Fig. 1), and the latter is outside the hydrographic boundary of the Great Basin (see Fig. 2.1 in Grayson, 2011). The two reconstructions of mean summer (current June to August) PDSI (Cook and Krusic, 2004) for grid nodes 71 (115.0° W, 40.0° N) and 72 (115.0° W, 37.5° N) were averaged together as they each covered a portion of the study area – plus several more Great Basin watersheds. Because of its biogeographical proximity, I also included the reconstructed Colorado River annual (from previous October to current September) streamflow at the Lees Ferry station (Meko et al., 2007), which closely resembles other, shorter reconstructions of discharge at the same location (Woodhouse and Lukas, 2006). The five

HESSD
10, 4301–4335, 2013

time series showed pairwise linear correlations around 0.6 (Table 3), with the exception of the Hughes and Graumlich (2000) reconstruction, which had the lowest values (0.2–0.3) when compared to the Utah (Gray et al., 2004) and Colorado River (Meko et al., 2007) ones. Overall, the reconstruction presented here was well correlated with all other ones, ranging from 0.5 with Hughes and Graumlich (2000) to 0.9 (the overall maximum) with Cook et al. (2004) PDSI record.

Information derived from the past, such as the tree-ring reconstructions I presented, requires careful consideration. On one hand, multi-century long proxy time series complement and expand the perspective derived from analysis of much shorter instrumental records and from projections of future scenarios (Pederson et al., 2012). This is made particularly clear by considering that regional climate model predictions on seasonal time scales have shown little skill outside of the tropical Pacific in non-ENSO years (Goddard et al., 2001), and even less skill may occur in multi-decadal regional climate projections (Pielke Sr. and Wilby, 2012). On the other hand, the numerical development of tree-ring chronologies and the statistical tools employed in most reconstructions are based on assumptions of linearity and stationarity (National Research Council, 2006). Although the line of organic correlation can generate more variable reconstructions than linear regression (Hirsch, 1982), the best current solution to the announced "death of stationarity" (Milly et al., 2008) lies in both an understanding of its true statistical meaning (Matalas, 2012) and in adopting a quantitative episode analysis to effectively place modern patterns into a long-term perspective. For instance, the early-1900s pluvial (Fye et al., 2004) was found repeatedly to be the most remarkable episode (sensu Biondi et al., 2005, 2008) during the past few centuries as well as throughout the Common Era, and this information is vital to realize the extent of the "wet bias" that affects the instrumental record of hydroclimatic variables in the Great Basin and the western USA in general.

Along the same lines, the 1930s "Dust Bowl" drought, which achieved top ten status in the episode analysis presented here, was much less prominent (falling to the 73rd position) in a 2300 yr precipitation reconstruction for the Walker River Basin, on the

HESSD
10, 4301–4335, 2013

east slope of the Sierra Nevada (Biondi et al., 2008). The current results confirm Strachan et al.'s (2012) finding that regional drought severity in the central Great Basin can differ from its realizations in the western portion of this region. Because the instrumental record better represents long-term hydro-climatic variability in the eastern portion of Nevada, near the Utah border, compared to its western portion, on the eastern slopes of the Sierra Nevada at the border with California, water management policies in eastern Nevada basins could more reliably use the 1920–1930's drought as a relevant scenario for extreme drought conditions. Since predicting changes in the statistics of regional climate over multi-annual time periods is essential to understand climate forcings and feedbacks, a similar approach could prove highly effective for individual sub-watersheds in other parts of the world. Multi-century long dendroclimatic records with km-scale spatial resolution are therefore essential tools for designing management practices with the objective to achieve drought resiliency in individual watersheds.

Acknowledgements. Research supported, in part, by Southern Nevada Water Authority, by the Office of the Vice President for Research at the University of Nevada, Reno, and by the US National Science Foundation under Cooperative Agreement EPS-0814372 and Grant No. P2C2-0823480. Completion of the article was allowed by a Visiting Fellowship from the Cooperative Institute for Research in the Environmental Sciences (CIRES) of the University of Colorado at Boulder. The views and conclusions contained in this document are those of the author and should not be interpreted as representing the opinions or policies of the funding agencies. I thank M. Cameletti, J. D. Salas, L. Saito, and J. Leising for helpful discussions of statistical and hydrological issues. I am also extremely grateful to the DendroLab personnel, especially Scotty Strachan, who contributed, either in the field or in the laboratory, to the development of the tree-ring network.

HESSD
10, 4301–4335, 2013

References

Abatzoglou, J., Diehl, H., Leising, J. F., Lutz, A., Redmond, K. T., and Thomas, J.: Evaluation of Climate Change Effects on Water Resources in Eastern Nevada, Desert Research Institute, Reno, NV, USA, 235 pp., 2012.

Antevs, E.: Rainfall and Tree Growth in the Great Basin, Carnegie Institution of Washington and American Geographical Society, New York, 97 pp., 1938.

Barnett, T. P. and Pierce, D. W.: When will Lake Mead go dry?, Water Resour. Res., 44, W03201, doi:10.1029/2007WR006704, 2008.

Barsugli, J. J., Nowak, K., Rajagopalan, B., Prairie, J. R., and Harding, B.: Comment on "When will Lake Mead go dry?" by T. P. Barnett and D. W. Pierce, Water Resour. Res., 45, W09601, doi:10.1029/2008WR007627, 2009.

Biondi, F.: Evolutionary and moving response functions in dendroclimatology, Dendrochronologia, 15, 139–150, 1997.

Biondi, F. and Qeadan, F.: Inequality in paleorecords, Ecology, 89, 1056–1067, 2008a.

Biondi, F. and Qeadan, F.: A theory-driven approach to tree-ring standardization: definining the biological trend from expected basal area increment, Tree-Ring Res., 64, 81–96, 2008b.

Biondi, F. and Strachan, S.: A *Pinus monophylla* tree-ring network for hydroclimatic studies in the Great Basin of North America, in: Abstracts of the 101st Annual Meeting of the Association of American Geographers, Special Session on "Dendrochronology II", Denver, Colorado, 2005.

Biondi, F. and Waikul, K.: DENDROCLIM2002: a C++ program for statistical calibration of climate signals in tree-ring chronologies, Comput. Geosci., 30, 303–311, 2004.

Biondi, F., Myers, D. E., and Avery, C. C.: Geostatistically modeling stem size and increment in an old-growth forest, Can. J. Forest Res., 24, 1354–1368, 1994.

Biondi, F., Kozubowski, T. J., and Panorska, A. K.: Stochastic modeling of regime shifts, Clim. Res., 23, 23–30, 2002.

Biondi, F., Kozubowski, T. J., and Panorska, A. K.: A new model for quantifying climate episodes, Int. J. Climatol., 25, 1253–1264, 2005.

Biondi, F., Kozubowski, T. J., Panorska, A. K., and Saito, L.: A new stochastic model of episode peak and duration for eco-hydro-climatic applications, Ecol. Model., 211, 383–395, 2008.

HESSD
10, 4301–4335, 2013

Biondi, F., Salas, J. D., Strachan, S., and Saito, L.: A dendrohydrological reconstruction for the Walker River Watershed (eastern Sierra Nevada/western Great Basin, USA) using new modeling techniques, in: 3rd USGS Modeling Conference, Special section on "High Resolution Models: Developments, Integration, and Applications", Denver, Colorado, 2010.
Box, G. E. P. and Jenkins, G. M.: Time Series Analysis: Forecasting and Control, Revised ed., Holden-Day, Oakland, 1976.
Brekke, L. D.: Addressing Climate Change in Long-Term Water Resources Planning and Management: User Needs for Improving Tools and Information, available at: http://www.usbr.gov/climate/userneeds/docs/LTdoc.pdf, last access: 3 April 2013, Technical Service Center, Bureau of Reclamation, Washington, DC, 2011.
Bunn, A. G., Korpela, M., Biondi, F., Campelo, F., Mérian, P., Qeadan, F., and Zang, C.: dplR: Dendrochronology Program Library in R, in: R package version 1.5.4, available at: http://CRAN.R-project.org/package=dplR (last access: 3 April 2013), 2012.
Cayan, D. R., Redmond, K. T., and Riddle, L. G.: ENSO and hydrological extremes in the western United States, J. Climate, 12, 2881–2894, 1999.
Christakos, G.: Modern Spatiotemporal Geostatistics, Oxford University Press, 2000.
Cole, K. L., Fisher, J., Arundel, S. T., Cannella, J., and Swift, S.: Geographical and climatic limits of needle types of one- and two-needled pinyon pines, J. Biogeogr., 35, 257–269, 2008.
Cook, E. R. and Kairiukstis, L. A.: Methods of Dendrochronology, Kluwer, Dordrecht, the Netherlands, 394 pp., 1990.
Cook, E. R. and Krusic, P. J.: The North American drought atlas, EOS T. Am. Geophys. Un., 84, GC52A-01, 2003.
Cook, E. R. and Krusic, P. J.: The North American Drought Atlas, Lamont-Doherty Earth Observatory, Palisades, NY, 2004.
Cook, E. R. and Peters, K.: The smoothing spline: a new approach to standardizing forest interior tree-ring width series for dendroclimatic studies, Tree-Ring Bull., 41, 45–53, 1981.
Cook, E. R., Woodhouse, C. A., Eakin, C. M., Meko, D. M., and Stahle, D. W.: Long-term aridity changes in the western United States, Science, 306, 1015–1018, 2004.
Cressie, N. A. C. and Wikle, C. K.: Statistics for Spatio-Temporal Data, Series in Probability and Statistics, Wiley, 2011.
Daly, C., Neilson, R. P., and Phillips, D. L.: A statistical-topographic model for mapping climatological precipitation over mountainous terrain, J. Appl. Meteorol., 33, 140–158, 1994.

HESSD
10, 4301–4335, 2013

Daly, C., Halbleib, M., Smith, J. I., Gibson, W. P., Doggett, M. K., Taylor, G. H., Curtis, J., and Pasteris, P. P.: Physiographically sensitive mapping of climatological temperature and precipitation across the conterminous United States, Int. J. Climatol., 28, 2031–2064, 2008.
Delwiche, L. D. and Slaughter, S. J.: The Little SAS Book: a Primer, 3rd Edn., SAS Institute Inc., Cary, NC, 2003.
Fassó, A. and Cameletti, M.: The EM algorithm in a distributed computing environment for modelling environmental space-time data, Environ. Modell. Softw., 24, 1027–1035, 2009.
Fassó, A. and Cameletti, M.: A unified statistical approach for simulation, modeling, analysis and mapping of environmental data, Simulation, 86, 139–154, 2010.
Fritts, H. C.: Tree Rings and Climate, Academic Press, London, UK, 567 pp., 1976.
Fritts, H. C. and Shatz, D. J.: Selecting and characterizing tree-ring chronologies for dendroclimatic analysis, Tree-Ring Bull., 35, 31–40, 1975.
Fye, F. K., Stahle, D. W., and Cook, E. R.: Paleoclimatic analogs to twentieth-century moisture regimes across the United States, B. Am. Meteorol. Soc., 84, 901–909, 2003.
Fye, F. K., Stahle, D. W., and Cook, E. R.: Twentieth-century sea surface temperature patterns in the Pacific during decadal moisture regimes over the United States, Earth Interact., 8, 1–22, doi:10.1175/1087-3562(2004)8¡1:TSSTPI¿2.0.CO;2, 2004.
Goddard, L., Mason, S. J., Zebiak, S. E., Ropelewski, C. F., Basher, R., and Cane, M. A.: Current approaches to seasonal-to-interannual climate predictions, Int. J. Climatol., 21, 1111–1152, 2001.
Gray, S. T. and McCabe, G. J.: A combined water balance and tree ring approach to understanding the potential hydrologic effects of climate change in the central Rocky Mountain region, Water Resour. Res., 46, W05513, doi:10.1029/2008WR007650, 2010.
Gray, S. T., Jackson, S. T., and Betancourt, J. L.: Tree-ring based reconstructions of interannual to decadal scale precipitation variability for northeastern Utah since 1226 AD, J. Am. Water Resour. Assoc., 40, 947–960, 2004.
Gray, S. T., Jackson, S. T., and Betancourt, J. L.: Uinta Basin Precipitation Reconstruction: IGBP PAGES/World Data Center for Paleoclimatology Data Contribution Series #2005-045, NOAA/NGDC Paleoclimatology Program, Boulder, CO, USA, 2005.
Grayson, D. K.: The Great Basin: a Natural Prehistory, Revised and Expanded Edition, University of California Press, Berkeley, CA, USA, 2011.
Grissino-Mayer, H. D.: Evaluating crossdating accuracy: a manual and tutorial for the computer program COFECHA, Tree-Ring Res., 57, 205–221, 2001.

HESSD
10, 4301–4335, 2013

Grissino-Mayer, H. D.: A manual and tutorial for the proper use of an increment borer, Tree-Ring Res., 59, 63–79, 2003.
Grissino-Mayer, H. D. and Fritts, H. C.: The international tree-ring data bank: an enhanced global database serving the global scientific community, Holocene, 7, 235–238, 1997.
Guisan, A. and Thuiller, W.: Predicting species distribution: offering more than simple habitat models, Ecol. Lett., 8, 993–1009, 2005.
Guttman, N. B. and Quayle, R. G.: A historical perspective of US climate divisions, B. Am. Meteorol. Soc., 77, 293–303, 1996.
Hardman, G. and Reil, O. E.: The Relationship Between Tree Growth and Stream Runoff in the Truckee River Basin, California-Nevada, Agricultural Experiment Station, University of Nevada, Reno, NV, 38 pp., 1936.
Helsel, D. R. and Hirsch, R. M.: Statistical methods in water resources, in: Techniques of Water-Resources Investigations of the United States Geological Survey, Chapter A3, United States Geological Survey, Reston, VA, 2002.
Hijmans, R. J., Cameron, S. E., Parra, J. L., Jones, P. G., and Jarvis, A.: Very high resolution interpolated climate surfaces for global land areas, Int. J. Climatol., 25, 1965–1978, 2005.
Hirsch, R. M.: A comparison of four streamflow record extension techniques, Water Resour. Res., 18, 1081–1088, 1982.
Hoerling, M. P., Lettenmaier, D. P., Cayan, D. R., and Udall, B.: Reconciling projections of Colorado River streamflow, Southwest Hydrol., 8, 20–21, 2009.
Holmes, R. L.: Computer-assisted quality control in tree-ring dating and measurement, Tree-Ring Bull., 43, 69–78, 1983.
Houghton, J. G., Sakamoto, C. M., and Gifford, R. O.: Nevada's Weather and Climate, Nevada Bureau of Mines and Geology, University of Nevada, Reno, NV, 78 pp., 1975.
Hughes, M. K. and Graumlich, L. J.: Climatic variations and forcing mechanisms of the last 2000 years, in: Multi-Millennial Dendroclimatic Studies from the Western United States, edited by: Bradley, R. S., Jones, P. D., and Jouzel, J., NATO ASI Series, Berlin, Germany, 109–124, 1996.
Hughes, M. K. and Graumlich, L. J.: Multi-millennial nevada precipitation reconstruction: IGBP PAGES/world data center – a for paleoclimatology data contribution series #2000-049, in: International Tree-Ring Data Bank, NOAA/NGDC Paleoclimatology Program, Boulder CO, USA, 2000.

HESSD
10, 4301–4335, 2013

Isaaks, E. H. and Srivastava, R. M.: An Introduction to Applied Geostatistics, Oxford University Press, New York, 1989.
Knight, T. A., Meko, D. M., and Baisan, C. H.: A bimillennial-length tree-ring reconstruction of precipitation for the Tavaputs Plateau, Northeastern Utah, Quaternary Res., 73, 107–117, 2010.
Knowles, N., Dettinger, M. D., and Cayan, D. R.: Trends in snowfall versus rainfall in the western United States, J. Climate, 19, 4545–4559, 2006.
Kyriakidis, P. C. and Journel, A. G.: Geostatistical space-time models: a review, Math. Geol., 31, 651–684, 1999.
Loaiciga, H. A., Haston, L., and Michaelsen, J.: Dendrohydrology and long-term hydrological phenomena, Rev. Geophys., 31, 151–171, 1993.
Matalas, N. C.: Comment on the announced death of stationarity, J. Water Res. Pl.-ASCE, 138, 311–312, 2012.
Meko, D. M., Woodhouse, C. A., Baisan, C. H., Knight, T., Lukas, J. J., Hughes, M. K., and Salzer, M. W.: Upper Colorado River Flow Reconstruction: IGBP PAGES/World Data Center for Paleoclimatology Data Contribution Series #2007-052, NOAA/NCDC Paleoclimatology Program, Boulder CO, USA, 2007.
Milly, P. C. D., Betancourt, J. L., Falkenmark, M., Hirsch, R. M., Kundzewicz, Z. W., Lettenmaier, D. P., and Stouffer, R. J.: Stationarity is dead: whither water management?, Science, 319, 573–574, 2008.
National Research Council: Surface Temperature Reconstructions for the Last 2000 Years, Committee on Surface Temperature Reconstructions for the Last 2000 Years, The National Academies Press, Washington, DC, 1–196, 2006.
National Research Council: Colorado River Basin Water Management: Evaluating and Adjusting to Hydroclimatic Variability, The National Academies Press, Washington, DC, 222 pp., 2007.
Nichols, W. D.: Reconstructed drought history, north-central Great Basin: 1601–1982, in: Aspects of Climate Variability in the Pacific and the Western Americas, edited by: Peterson, D. H., Geophysical Monograph, 55, American Geophysical Union, Washington, DC, USA, 61–67, 1989.
Pebesma, E.: Spatio-temporal geostatistics using gstat, R Foundation for Statistical Computing, Müster, Germany, 1–11, 2013.

HESSD
10, 4301–4335, 2013

Pederson, N., Bell, A. R., Knight, T. A., Leland, C., Malcomb, N., Anchukaitis, K. J., Tackett, K., Scheff, J., Brice, A., Catron, B., Blozan, W., and Riddle, J.: A long-term perspective on a modern drought in the American Southeast, Environ. Res. Lett., 7, 014034, doi:10.1088/1748-9326/7/1/014034, 2012.

Pielke Sr., R. A. and Wilby, R. L.: Regional climate downscaling – what's the point?, EOS Forum, EOS Trans. Am. Geophys. Union, 93, 52–53, doi:10.1029/2012EO050008, 2012.

Prairie, J. R., Nowak, K., Rajagopalan, B., Lall, U., and Fulp, T.: A stochastic nonparametric approach for streamflow generation combining observational and paleoreconstructed data, Water Resour. Res., 44, W06423, doi:10.1029/2007WR006684, 2008.

Rajagopalan, B., Nowak, K., Prairie, J. R., Hoerling, M. P., Harding, B., Barsugli, J. J., Ray, A., and Udall, B.: Water supply risk on the Colorado River: can management mitigate?, Water Resour. Res., 45, W08201, doi:10.1029/2008WR007652, 2009.

R Development Core Team: R: a language and environment for statistical computing, 2.15.0 Edn., R Foundation for Statistical Computing, Vienna, Austria, 2012.

Redmond, K. T., Enzel, Y., House, K. P., and Biondi, F.: Climate variability and flood frequency at decadal to millennial time scales, in: Ancient Floods, Modern Hazards: Principles and Applications of Paleoflood Hydrology, edited by: House, K. P., Webb, R. H., Baker, V. R., and Levish, D. R., Water Science and Application, American Geophysical Union, Washington, DC, 21–45, 2002.

Romme, W. H., Allen, C. D., Bailey, J. D., Baker, W. L., Bestelmeyer, B. T., Brown, P. M., Eisenhart, K. S., Floyd, M. L., Huffman, D. W., Jacobs, B. F., Miller, R. F., Muldavin, E. H., Swetnam, T. W., Tausch, R. J., and Weisberg, P. J.: Historical and modern disturbance regimes, stand structure, and landscape dynamics in piñon-juniper vegetation of the Western United States, Rangeland Ecol. Manage., 62, 203–222, doi:10.2111/08-188R1.1, 2009.

Salas, J. D., Raynal, J. A., Tarawneh, Z. S., Lee, T. S., Frevert, D., and Fulp, T.: Extending short records of hydrologic data, in: Hydrology and Hydraulics, edited by: Singh, V. P., Water Resources Publications, LLC, Highlands Ranch, CO, 717–760, 2008.

Seager, R., Ting, M. F., Held, I. M., Kushnir, Y., Lu, J., Vecchi, G., Huang, H.-P., Harnik, N., Leetmaa, A., Lau, N.-C., Li, C., Velez, J., and Naik, N.: Model projections of an imminent transition to a more arid climate in southwestern North America, Science, 316, 1181–1184, 2007.

Smith, W. P.: Reconstruction of precipitation in northeastern Nevada using tree rings, 1600–1982, J. Clim. Appl. Meteorol., 25, 1255–1263, 1986.

HESSD
10, 4301–4335, 2013

Speer, J. H.: Fundamentals of Tree-Ring Res., University of Arizona Press, Tuscon, 333 pp., 2010.
Stahle, D. W., Cook, E. R., Cleaveland, M. K., Therrell, M. D., Meko, D. M., Grissino-Mayer, H. D., Watson, E., and Luckman, B. H.: Tree-ring data document 16th century megadrought over North America, EOS T. Am. Geophys. Un., 81, 121–125, 2000.
Stakhiv, E. Z.: Pragmatic approaches for water management under climate change uncertainty, J. Am. Water Resour. Assoc., 47, 1183–1196, 2011.
Stewart, I. T., Cayan, D. R., and Dettinger, M. D.: Changes in snowmelt runoff timing in western North America under a "business as usual" climate change scenario, Climatic Change, 62, 217–232, 2004.
Stokes, M. A. and Smiley, T. L.: An Introduction to Tree-Ring Dating, Reprint of 1968 U. of Chicago Press Edn., University of Arizona Press, Tucson, AZ, USA, 73 pp., 1996.
Strachan, S., Biondi, F., and Leising, J.: A 550-year reconstruction of streamflow variability in Spring Valley, Nevada, USA, J. Water Res. Pl.-ASCE, 138, 326–333, doi:10.1061/(ASCE)WR.1943-5452.0000180, 2012.
Tabios III, G. Q. and Salas, J. D.: A comparative analysis of techniques for spatial interpolation of precipitation, Water Resour. Bull., 21, 365–380, 1985.
West, N. E. and Young, J. A.: Intermountain valleys and lower mountain slopes, in: North American Terrestrial Vegetation, 2nd Edn., edited by: Barbour, M. G. and Billings, W. D., Cambridge University Press, Cambridge, UK, 255–284, 2000.
Wilby, R. L.: A review of climate change impacts on the built environment, Built Environ., 33, 31–45, 2007.
Woodhouse, C. A. and Lukas, J. J.: Multi-century tree-ring reconstructions of Colorado streamflow for water resource planning, Climatic Change, 78, 293–315, 2006.

HESSD
10, 4301–4335, 2013

Table 1. Summary of 22 single-leaf pinyon tree-ring chronologies generated from the measured ring-width series according to Eq. (1)*. Site locations are mapped in Fig. 1, and time-series plots of the chronologies are shown in Fig. 2.

SITE	Site name	Elev. (m)	Max (yr)	No. rings	LAR	LAR (%)	T	S	MSL (yr)	First/last year	Mean index	Min/max index	St. dev.	G	A_1
Bri	Bristol Range	2340	347	8274	124	1.5	15	30	276	1650/2008	0.975	0.003/1.859	0.292	0.166	0.161
Con	Connors Summit	2430	418	11177	159	1.4	18	33	339	1600/2007	0.986	0.003/1.771	0.308	0.176	0.267
Djm	Dutch John Mt	2060	378	5159	134	2.6	8	16	322	1636/2007	0.975	0.003/1.831	0.384	0.221	0.033
Ggm	Golden Gate Range	2350	498	5343	160	3.0	10	16	334	1530/2007	0.978	0.002/2.062	0.375	0.215	0.299
Ker	Kern Mts, West	2300	493	11128	469	4.2	15	28	397	1527/2008	0.980	0.002/2.327	0.467	0.269	0.193
Mti	Mt. Irish Range	2390	703	7907	278	3.5	11	18	439	1373/2003	0.971	0.003/1.910	0.339	0.194	0.224
Sca	Schell Creek Range, Central	2260	588	12767	303	2.4	20	40	319	1447/2007	0.981	0.002/1.780	0.340	0.194	0.121
Scc	Schell Creek Range, South	2280	667	13063	522	4.0	19	31	421	1374/2007	0.977	0.002/2.260	0.381	0.217	0.213
Sck	Snake Range, South	2360	485	8720	181	2.1	14	25	349	1473/2002	0.983	0.002/2.176	0.320	0.180	0.239
Sna	Snake Range, North	2400	784	14030	770	5.5	20	37	379	1327/2007	0.975	0.002/2.203	0.464	0.271	0.172
Svb	Wilson Creek Range	1930	433	7857	101	1.3	17	33	238	1537/2007	0.982	0.002/1.777	0.318	0.182	0.232
Svc	White Rock Mts., Site 1	2350	558	12455	256	2.1	21	38	328	1470/2007	0.977	0.003/1.904	0.314	0.178	0.204
Svd	White Rock Mts., Site 2	2160	578	15700	185	1.2	26	52	302	1529/2007	0.977	0.003/1.873	0.296	0.168	0.274
Sve	White Rock Mts., Site 3	2130	442	9836	154	1.6	19	36	273	1554/2007	0.983	0.003/1.677	0.301	0.171	0.139
War	Egan Range, Central	2170	549	10513	307	2.9	14	26	404	1479/2008	0.976	0.003/2.053	0.352	0.202	0.307
Whr	White Pine Range, South	2250	603	4581	204	4.5	11	13	352	1512/2002	0.974	0.001/2.438	0.409	0.232	0.201
Wpn	White Pine Range, North	2220	719	16830	542	3.2	18	38	443	1296/2008	0.978	0.003/1.933	0.355	0.203	0.172
365	Egan Range West	2134	512	7033	175	2.5		27	261	1603/1976	0.975	0.003/2.241	0.375	0.216	0.187
460	Berry Creek	2242	426	8062	117	1.5		42	192	1630/1976	0.978	0.002/2.035	0.377	0.218	0.345
HCR	Horse Canyon Ridge	2347	412	7760	215	2.8		24	323	1596/1978	0.980	0.003/1.974	0.368	0.212	0.159
MDY	Moody Mountain	2004	533	11576	409	3.5		42	276	1520/1982	0.969	0.002/2.326	0.417	0.243	0.302
PAN	Panaca Summit	2103	325	9494	143	1.6		48	198	1612/1982	0.982	0.003/1.850	0.346	0.199	0.245

* The summary includes values that are based on all measured ring-width series for a site, regardless of standardization option, such as Max = number of years in the longest series, which is an index of the maximum tree age at each site; No. Rings = total number of crossdated and measured tree rings; LAR = number of locally absent rings; LAR (%) = percentage of "No. Rings" equal to zero (which is the conventional value for a LAR); T = number of sampled trees (for the five ITRDB sites, this value was not available); S = number of ring-width series; MSL = mean series length.
Other values (columns to the right of MSL) depend on the standardization option (expressed as a formula for clarity) and are calculated from the master tree-ring chronology for a site, such as G = Gini coefficient, a measure of all-lag variability (Biondi and Qeadan, 2008a); A_1 = first-order autocorrelation, a measure of persistence (Box and Jenkins, 1976).

HESSD
10, 4301–4335, 2013

Table 2. The 10 "strongest" episodes identified in the 327 yr (1650–1976) average proxy record of October–May precipitation anomalies (see Fig. 9 for a time series plot). Ranking* was done for (A) the 150 episodes identified by the annual mean (black line in Fig. 9), and (B) the 55 episodes identified by the 7.5 yr spline smoothing (red line in Fig. 9).

(A) Start (year)	End (year)	Episode Type	Duration (years)	Absolute Magnitude (mm)	Absolute Maximum (mm)	Score
1905	1915	Pos	11	589	140	444
1876	1883	Neg	8	357	150	440
1723	1728	Pos	6	470	156	438
1706	1710	Neg	5	423	132	428
1751	1757	Neg	7	418	110	427
1848	1855	Pos	8	330	107	424
1780	1783	Neg	4	326	171	420
1933	1936	Neg	4	303	181	418
1837	1840	Pos	4	358	125	414
1856	1861	Neg	6	267	117	413

(B) Start (year)	End (year)	Episode Type	Duration (years)	Absolute Magnitude (mm)	Absolute Maximum (mm)	Score
1904	1924	Pos	21	836.2	73	161
1925	1937	Neg	13	373.7	70	154
1703	1711	Neg	9	421.8	90	153
1776	1784	Neg	9	382.0	74	150
1946	1964	Neg	19	381.0	46	142
1750	1757	Neg	8	357.1	63	139
1692	1702	Pos	11	354.9	50	137
1855	1864	Neg	10	298.5	56	137
1876	1883	Neg	8	290.7	63	134
1723	1728	Pos	6	358.2	97	133

* Positive (Pos) episodes indicate wet periods, negative (Neg) episodes indicate dry periods. The three episode parameters (duration, absolute magnitude, and absolute maximum) were separately ranked (with increasing ranks for increasing values), and the three ranks were added to obtain the final score (the higher the score, the stronger the episode).

HESSD
10, 4301–4335, 2013

Table 3. Pairwise linear correlation coefficients computed between five dendroclimatic reconstructions for the period 1650–1976.

	MAP_M	H&G1996	G&a2004	M&a2007
H&G1996	0.548			
G&a2004	0.582	0.230		
M&a2007	0.584	0.297	0.643	
C&a2004	0.886	0.536	0.631	0.656

* MAP_M = average of 315 grid-point reconstructions of total October–May precipitation anomalies (see Fig. 9).
H&G1996 = total annual (from previous July to current June) precipitation for Nevada Climate Division 3.
G&a2004 = total annual (from previous June to current June) precipitation for Utah Climate Division 6.
M&a2007 = Colorado River annual (from previous October to current September) streamflow at the Lees Ferry station.
C&a2004 = mean summer (current June to August) PDSI for grid nodes 71 and 72.

HESSD
10, 4301–4335, 2013

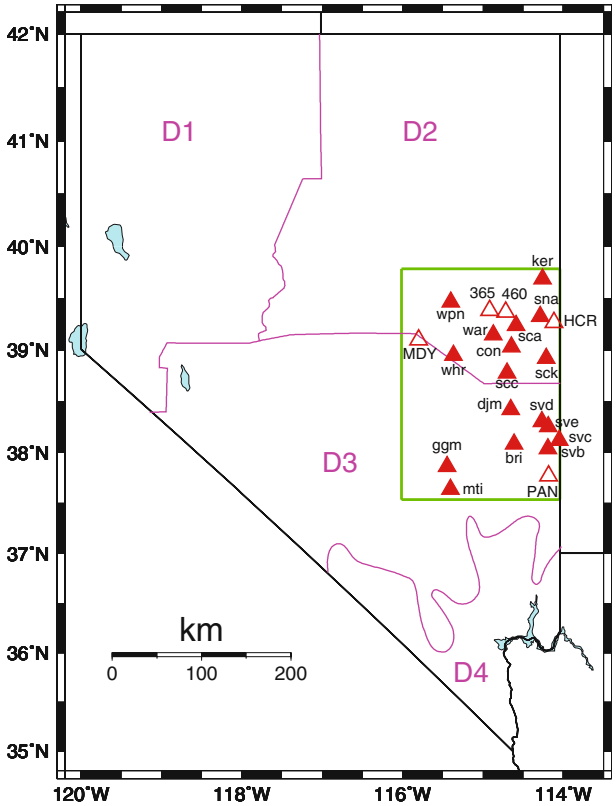

Fig. 1. Map of the tree-ring chronologies (red triangles, solid for new sites and empty for ITRDB sites) used to reconstruct October–May total precipitation. The boundaries of the four Nevada Climate Divisions (violet) and of the area used to define the 12 km grid points (green) are also shown. Site IDs are the same as in Table 1.

HESSD
10, 4301–4335, 2013

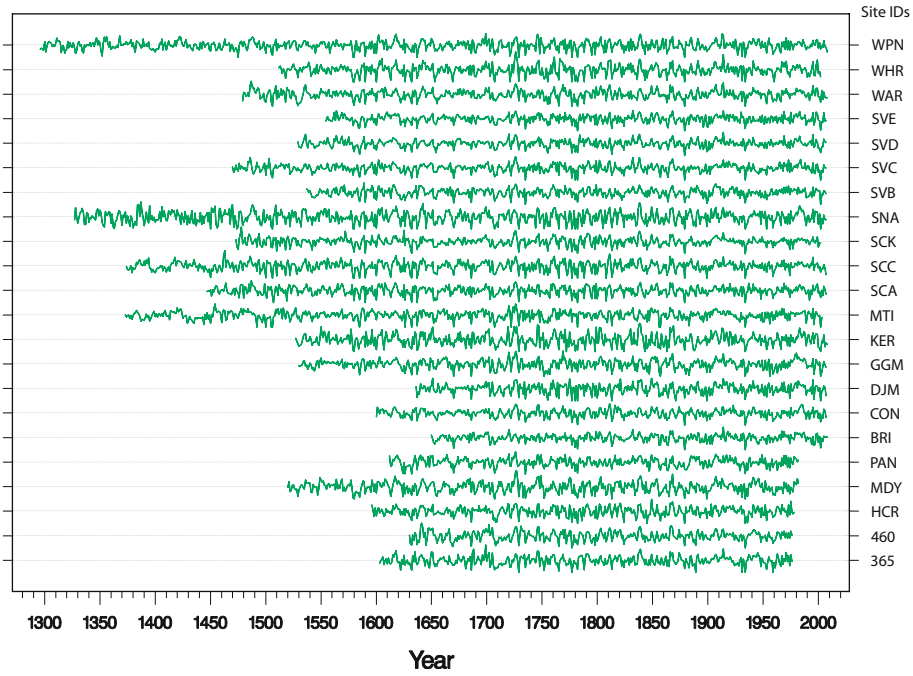

Fig. 2. Time-series patterns of 22 tree-ring chronologies derived from single-leaf pinyon samples. Series were plotted using a constant scale; a dotted line was used to represent their long-term mean. Site IDs are the same as in Table 1; the five ITRDB chronologies are plotted in the lower portion of the graph, and end about 30 yr earlier than the rest.

HESSD
10, 4301–4335, 2013

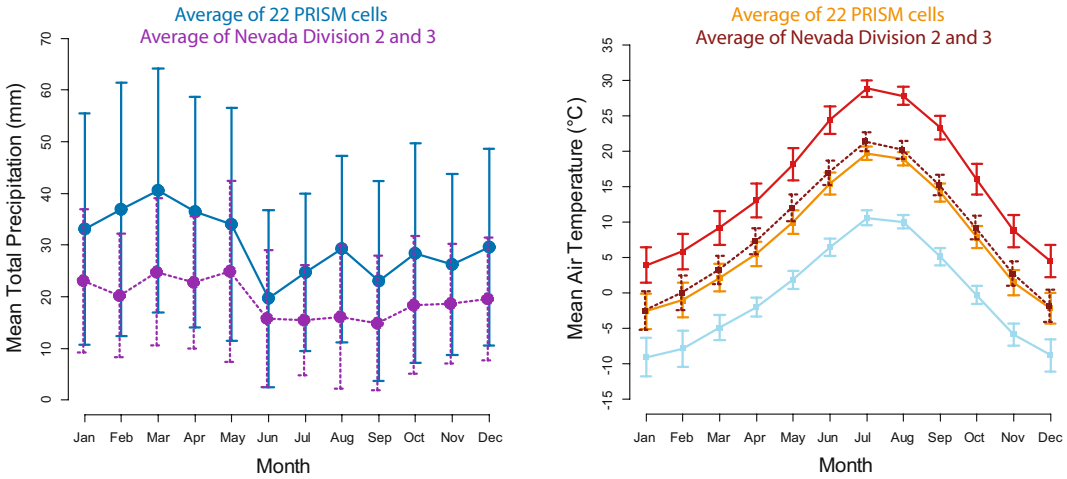

Fig. 3. Annual cycle of monthly climate variables showing the mean (circles for precipitation, squares for temperature) ± 1 standard deviation (bars) computed using all available years (1895–2006). Monthly maximum (red) and minimum (cyan) temperatures from PRISM data were averaged to obtain monthly mean (orange) temperature. Values obtained by combining the 22 PRISM grid cells that include a tree-ring site are shown with solid lines; values obtained by combining Climate Division 2 and 3 data are shown with dashed lines, as well as different colors (and a slight horizontal offset).

HESSD
10, 4301–4335, 2013

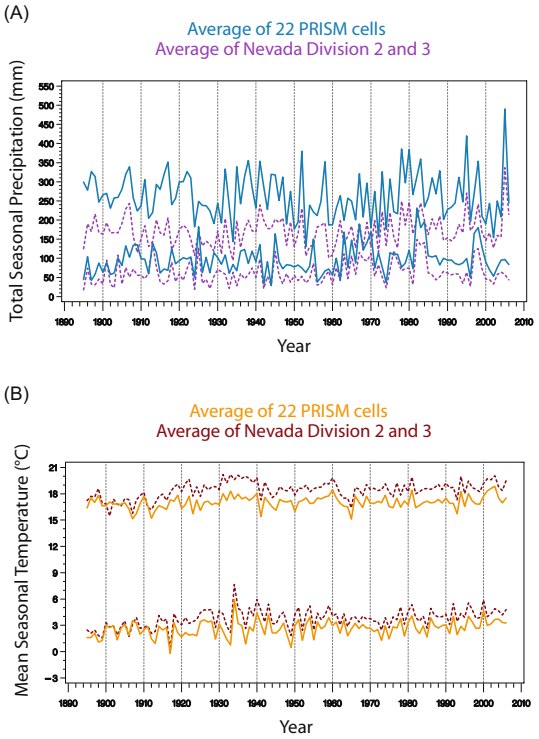

Fig. 4. Time-series graph of seasonal climate variables from 1895 to 2006. Monthly maximum and minimum temperatures from PRISM data were averaged to obtain monthly mean temperature. Values obtained by combining the 22 PRISM grid cells that include a tree-ring site are shown with solid lines; values obtained by combining Climate Division 2 and 3 data are shown with dashed lines, as well as different colors (same color scheme as in Fig. 3). **(A)** Upper curves (denim blue for PRISM, purple for Climate Division data) are for October–May, lower curves are for June–September. **(B)** Upper curves are for June–September, lower curves are for October–May.

HESSD
10, 4301–4335, 2013

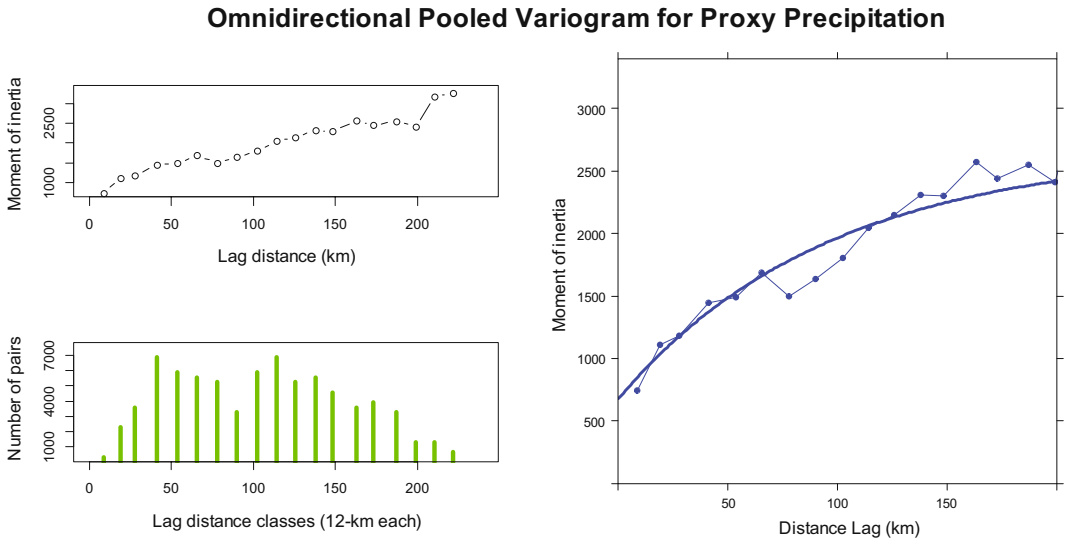

Fig. 5. Pooled variogram (left panels: estimated gamma values and number of pairs for each 12 km distance class; right panel: exponential model fit to the estimated gamma values) for the 327 yr of the 22 site reconstructions of October–May total precipitation anomalies.

HESSD
10, 4301–4335, 2013

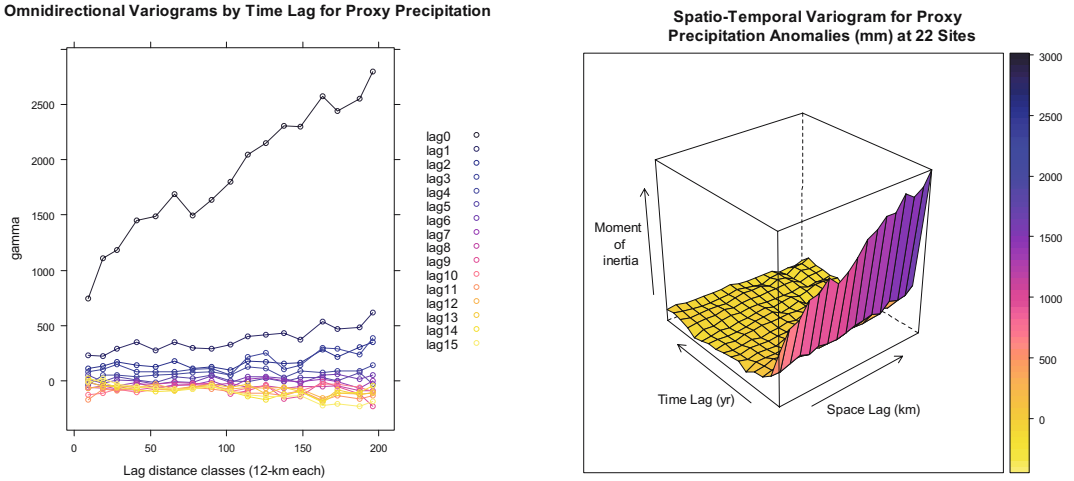

Fig. 6. Temporally lagged variograms (estimated gamma values for each 12 km distance class) for the 327 yr of the 22 site reconstructions of October–May total precipitation anomalies. Left panel: the deviation from a horizontal line (= no spatial continuity) shows that most of the spatial dependence is found at lag zero, and little spatial dependence remains at time lags greater than one year. Right panel: a three-dimensional plot, showing the much greater spatial dependence compared to the temporal one.

HESSD
10, 4301–4335, 2013


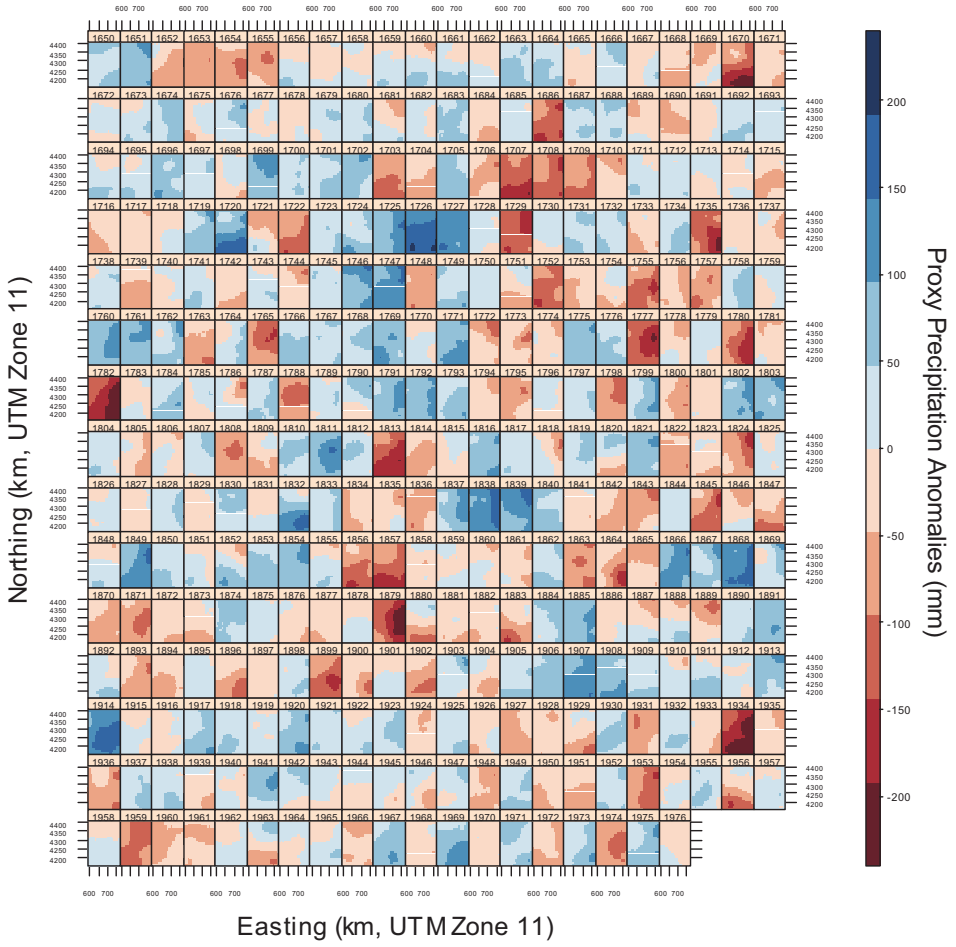

Fig. 7. Pseudo-color annual maps of spatio-temporal kriging estimates for October–May total precipitation anomalies (mm) over the 327 yr record.

HESSD
10, 4301–4335, 2013

Space-time kriging extension of precipitation variability

F. Biondi

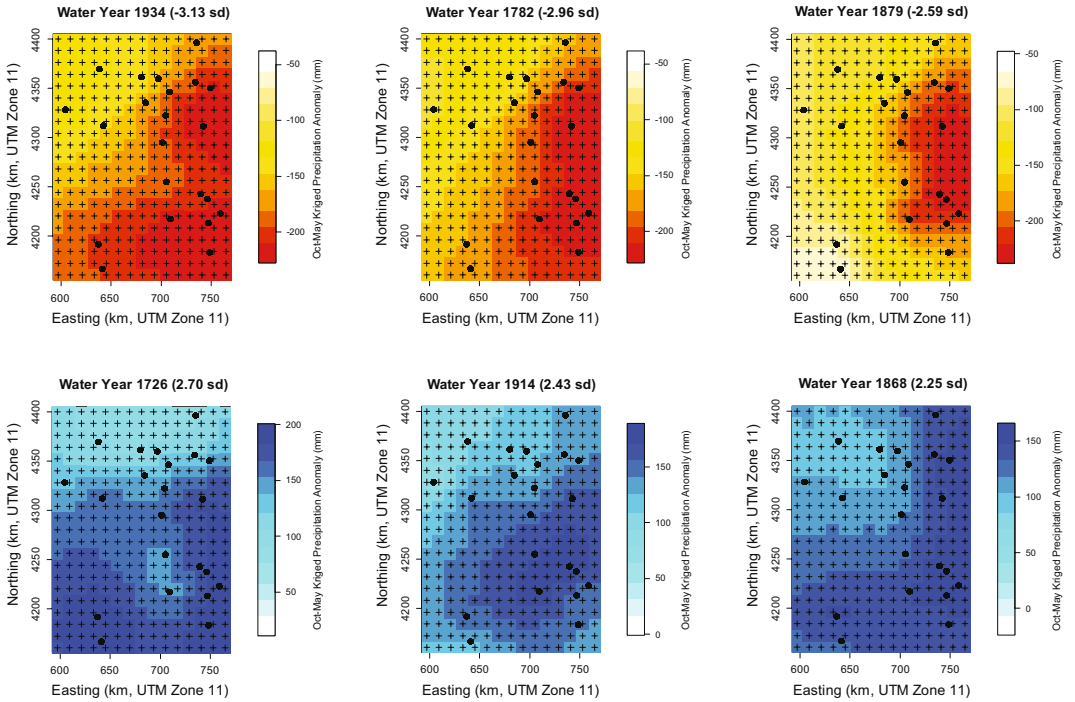

Fig. 8. Pseudo-color maps of spatio-temporal kriging estimates for (top row) the three driest years (1934, 1782, and 1879) and (bottom row) the three wettest years (1726, 1914, and 1868) in the 1650–1976 proxy record of October–May total precipitation anomalies. The location of tree-ring chronologies (solid black circles) and 12 km grid points (black crosses) is also shown. Note that these color palettes have slightly different end points but constant range (190 mm), hence differences in pseudo-color patterns matched those in actual kriged estimates, showing that spatial variability was generally higher in wet years than in dry ones.

HESSD
10, 4301–4335, 2013

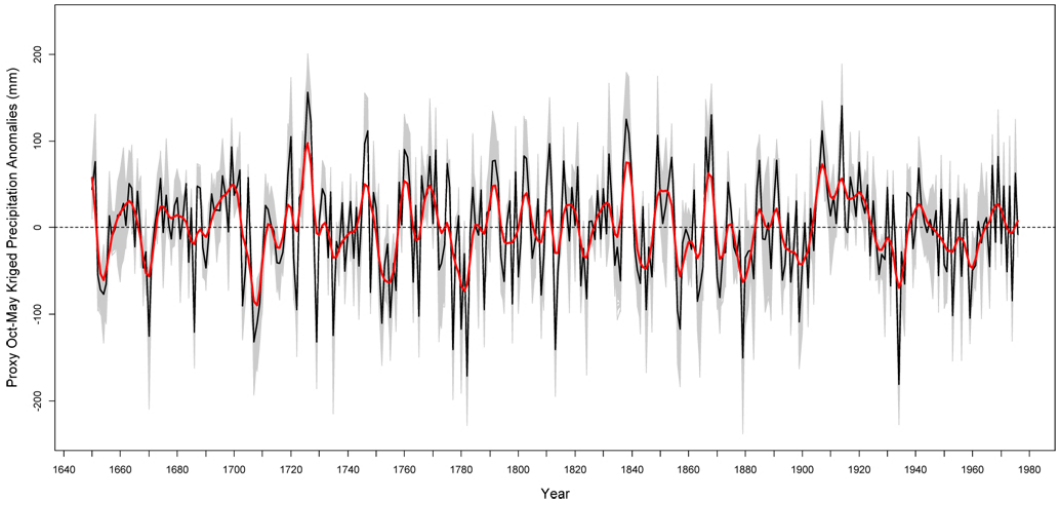

Fig. 9. Time-series plot of the October–May total precipitation anomalies (mm) averaged from the 315 kriged grid-point proxy records. Annual patterns (gray lines) were overlaid to show the overall variability; the mean of all series (black line) was fit with a 7.5 yr cubic smoothing spline (red line) to show interannual patterns at ENSO timescales. Wet (i.e., positive) and dry (i.e., negative) episodes are above or below the zero reference level (dashed line). It is easy to notice the unique early 1900s pluvial (i.e., wet period) compared to the previous three centuries.

HESSD
10, 4301–4335, 2013